KUNS 1314
December 1994

Reaction Cross Sections in Light Nuclear Systems with the Multiconfiguration Resonating-Group Method

YOSHIKAZU FUJIWARA

Department of Physics, Kyoto University, Kyoto 606-01, Japan

and

Y. C. TANG

School of Physics, University of Minnesota, Minneapolis, Minnesota 55455, USA

ABSTRACT

Differential cross sections for various reactions in the 6-, 7-, 8- and 10-nucleon systems, obtained by using multiconfiguration resonating-group calculations, are compared with experimental results. These comparisons show that the calculation can explain quite well the general features of the measured angular distributions, such as the cross-section rise at backward angles, the angular positions of cross-section maxima and minima, and so on. Discrepancies with experiment, none serious, can all be readily and satisfactorily explained. These findings, together with previous discussions on level spectra and scattering cross sections, indicate that there is now enough evidence to confidently support the assertion that the resonating-group method is a sound microscopic method built on firm physical foundation, and can be successfully used to treat nuclear bound-state, scattering, and reaction problems from a unified and consistent viewpoint.

1. Introduction

The resonating-group method [1,2] (RGM) is a microscopic method which has the important feature of treating nuclear bound-state, scattering, and reaction problems in a unified manner. In the application of this method to a particular nuclear system, one chooses a model space that is spanned by a number of cluster configurations selected appropriately by physical intuition, energetical arguments, and relative ease in analytical derivation, and adopts a nucleon-nucleon potential that explains satisfactorily the two-nucleon low-energy scattering data. The reliability of the results obtained can be gauged by comparing the calculated total reaction cross sections with measured values. For instance, in the 6-nucleon case performed in a model space consisting of $d+\alpha$, $p+^5$He, $n+^5$Li and pseudo-inelastic configurations involving deuteron pseudo-excited states, the calculated $d+\alpha$ total reaction cross section at a c.m. energy of 22 MeV is equal to 294 mb,[3] which compares very well with the measured value of 309 mb.[4] This favorable comparison suggests that, with these chosen cluster configurations, the 6-nucleon calculation is performed in a large enough model space, and can be considered to be essentially complete. Thus, one can confidently make use of the calculated results for energy spectra, scattering and reaction cross sections to achieve a basic understanding of the important properties of this light nuclear system. Similarly, we have studied recently the 7-, 8- and 10-nucleon systems with the multiconfiguration RGM. [5-7] There we found that the calculated total reaction cross sections turn out to be in excess of 70% of the measured values. Therefore, these calculations can also be used to demonstrate the RGM feature of a unified description of nuclear bound-state, scattering, and reaction phenomena.

The theoretical energy spectra of bound and resonance states obtained in the 6, 7, 8 and 10-nucleon systems [5,6,8,9] agree well with experimental observation. As an example, we mention the situation in ^{8}Li where it was found that the calculated and empirical level spectra have a good correspondence for all low-lying states. [6] This suggests rather convincingly that the multiconfiguration RGM cal-

culation performed in this system contains most of the essential ingredients. In the case of scattering, we have also obtained quite reasonable results. It is shown in Refs. 3), 5), 6) and 9) that the calculation yields all the oscillatory features of the measured angular distributions. In particular, the large cross-section rise at backward directions, occurring especially in systems such as $d + \alpha$, $^3\mathrm{He} + \alpha$ and $\alpha + {}^6\mathrm{Li}$ where the nucleon-number difference of the interacting nuclei is small, is nicely explained. This latter feature occurs, of course, mainly as a consequence of the fact that totally antisymmetric wave functions are used in RGM calculations and, hence, core-exchange effects are fully taken into account.

Differential reaction cross sections calculated in the 6-, 7-, 8- and 10-nucleon systems will be discussed in this paper. We decide to show the results from these different systems collectively, because it is our opinion that such a joint presentation will demonstrate in a more convincing manner the unifying nature of RGM calculations. In addition, it should be mentioned that some of the results published previously were obtained with a phase error in the computation, which is related to the time-reversal property of the chosen angular-momentum function. Fortunately, in three-cluster problems of s-shell clusters without noncentral forces, it turns out that the calculated partial and total reaction cross sections are not at all affected by this error, and only differential scattering and reaction cross sections involving incoming and outgoing channels with two-cluster subsystems having non-zero relative orbital angular momentum (i.e., $I \neq 0$) need to be modified. Thus, the results requiring modifications are those for $^4\mathrm{He}(d,p)^5\mathrm{He}$ reaction shown in Fig. 6 of Ref. 3), those for $^4\mathrm{He}(^3\mathrm{He},p)^6\mathrm{Li}^*$, $^4\mathrm{He}(^3\mathrm{He},d)^5\mathrm{Li}$, $^6\mathrm{Li}(n,n')^6\mathrm{Li}^*$, and $^6\mathrm{Li}(n,d)^5\mathrm{He}$ reactions shown in Figs. 11 and 15 of Ref. 5), and those for $n + {}^7\mathrm{Li}$ elastic scattering shown in Fig. 18 of Ref. 6). In this paper, the corrected results will also be presented.

It is interesting to mention that, aside from our results to be discussed here, the number of microscopic reaction calculations performed in large model spaces is, in fact, fairly small. Beyond the 3-nucleon system, there seem to exist only this type of calculations in 4- and 5-nucleon systems, [10,11] and some brief discussion in the

7-nucleon case. [12] Therefore, our series of systematic reaction calculations in the 6-, 7-, 8- and 10-nucleon systems is important, and should serve to substantially promote the case for the use of microscopic considerations in studying the essential properties of nuclear reactions.

Since the 3-cluster coupled-rearrangement-channel formalism used in the 6-, 7-, 8- and 10-nucleon calculations has already been described in our previous publications, [2] we shall mention in §2 only some points concerning the model spaces and the nucleon-nucleon potential that are essential to our discussion. In §3, we will present the results obtained for the differential cross sections of various reactions occurring in these four systems. Comparison with experiment will also be made here in order to demonstrate the usefulness of the microscopic approach. Finally, in §4, we make some concluding remarks and discuss the improvements that seem to be still necessary, particularly with regard to the extension of the chosen model space.

2. Brief review of the formulation

Cluster configurations used in the calculations are listed in Table I, where PIC denotes pseudo-inelastic configurations involving pseudo-excited states of the deuteron. From this table, one sees that the number of 2-cluster configurations in each of the considered systems is rather large. As an inevitable consequence of this, the computational requirements become quite severe. To partially overcome this difficulty, we have chosen to simplify the calculation by using a purely central nucleon-nucleon potential without Coulomb and noncentral components. In fact, this is a rather practical simplification to make in a systematic investigation of a number of nuclear systems, because this simplification does not generally affect in any serious manner the essential characteristics of the calculated differential scattering and reaction cross sections, but has the added advantage that the interpretation of the calculated results becomes sufficiently simple to enable one to

extract useful information about the important mechanisms which take place in nuclear reactions. [2)]

The nucleon-nucleon potential used is the Minnesota or MN potential given by Eqs. (4) - (6) of Ref. 2) (see also Ref. 13)). It contains a soft repulsive core, and was designed to fit the two-nucleon effective-range parameters and to yield reasonable values for the binding energies and rms radii of the 2-, 3- and 4-nucleon clusters which are the essential building blocks in a microscopic cluster theory. The exchange-mixture parameter u contained in this potential is an adjustable quantity and is chosen by using the bound-state information in the nuclear system under consideration. The resultant values are also given in Table I. Here one notes that the values of u in the 6-, 7- and 8-nucleon systems are nearly the same,* but that in the 10-nucleon system is significantly lower. The fact that the u-values in the three lower-A systems turn out to be similar is likely coincidental and should not be taken too seriously. At present, there exist indications that the model space employed in the 6-nucleon calculation is very probably large enough, but the model spaces adopted in the 7-, 8- and 10-nucleon calculations may not be sufficiently extensive. This means that, if we further expand the model spaces in these three latter systems, the u-values would turn out to be somewhat smaller. Thus, what we really find here is that there is a general tendency for the value of u to decrease as the nucleon number of the system increases. This is actually not unexpected, but is a reflection of the fact that our chosen nucleon-nucleon potential has only a weakly repulsive core and, hence, is not sufficiently saturating. Indeed, in the investigations of the $N + \alpha$, $N + {}^{16}\mathrm{O}$, and $N + {}^{40}\mathrm{Ca}$ systems, [13)] a similar trend has also been observed.

Since the adequacy of the chosen model space is gauged by the calculated total

$\star$ The u-values given in Table I for the 7- and 8-nucleon systems are slightly too large. To obtain correctly the ${}^3\mathrm{H}+\alpha$ separation energy in the lowest $(L,S) = (1,1/2)$ state of ${}^7\mathrm{Li}$ and the $n+{}^7\mathrm{Li}$ separation energy in the $(L,S) = (1,0)$ first-excited state of ${}^8\mathrm{Li}$, one should use a u-value very close to 0.98 in both of these systems. It should be emphasized, however, that such a small reduction in u-value will not change the main characteristics of the scattering and reaction angular-distribution curves, and will affect only in a rather minor manner the quality of comparison between calculation and experiment.

reaction cross section σ_R, we review in Table II the results for σ_R obtained in the 6-, 7-, 8- and 10-nucleon cases. In this table, comparisons with experimental values are also shown, except in the 10-nucleon case where the calculated value is compared with an empirical value obtained from a single-configuration $\alpha + {}^6\mathrm{Li}$ resonating-group study in which reaction effects are taken into account by the inclusion of a phenomenological imaginary potential in the formulation. [19)] Because this latter comparison is obviously rather indirect, we are inclined to believe that the ratio ρ of calculated to experimental values of σ_R in the 10-nucleon system is likely to be not as reliable as those in the other lower-A systems.

In the 6-nucleon system, the calculated $d+\alpha$ total reaction cross sections at 10 and 22 MeV exceed 90% of the experimental values. Thus, as is mentioned in §1, the model space used in this system is large enough, and the calculated differential scattering and reaction cross sections should turn out to be satisfactory. The situations in the 7-, 8- and 10-nucleon systems are somewhat different. Here the calculated total reaction cross sections are equal to 70 - 80 % of the experimental values. This indicates that a further improvement in the formulation of these systems will still be desirable. On the other hand, the comparison between calculated and experimental σ_R is already reasonably favorable, suggesting that the calculated differential scattering and reaction cross sections should explain most of the important features of the measured results.

3. Differential reaction cross-section results

3.1. General discussion

Before we describe the features of the calculated differential reaction cross sections, we wish to discuss the following factors which influence the quality of comparison between calculation and experiment:

(a) When the chosen model space is not sufficiently extensive, the calculated total reaction cross section will be too small, but the calculated differential scattering and reaction cross sections will generally be overestimated. The reason for this

is quite simple, and is related to the fact that not enough flux is drained off from the incident channel in such a situation. On the other hand, one does expect that the diffraction and interference features exhibited in cross-section angular distributions will essentially be maintained, especially in light nuclear systems. In making this assertion, we are relying not only on experience that was obtained in calculations with phenomenological imaginary potentials (see, e.g., Fig. 1 of Ref. 20)), but also on experience that we acquired from multiconfiguration resonating-group studies themselves. To illustrate this latter point, we show in Figs. 1 and 2 the cross-section angular distributions of $n + {}^7\mathrm{Li}$ scattering and ${}^7\mathrm{Li}(n,n'){}^7\mathrm{Li}^*$ reaction at 12.2 MeV in various model spaces. In these figures, the symbol SC denotes results obtained with the $n + {}^7\mathrm{Li}$ cluster configurations only, while the symbols DC2, TC, and QC represent results obtained by successively adding the cluster configurations $n + {}^7\mathrm{Li}^*$, $t + {}^5\mathrm{He}$, and ${}^4\mathrm{H} + \alpha$. By studying these figures, one can conclude with reasonable confidence that the above-mentioned assertion is indeed rather well supported. Even in the ${}^7\mathrm{Li}(n,n'){}^7\mathrm{Li}^*$ reaction case, it is noted that the differences between the TC and QC results occur mainly in the magnitude of the cross section, but not in the oscillatory feature of the angular distribution.

(b) In a reaction $A(a,b)B$, the cluster B is usually specified by non-zero values for the internal orbital angular momentum I and the spin angular momentum S. Because the nucleon-nucleon potential contains non-central components, this (I,S) state will split into a number of energetically separated levels with different values for the total angular momentum J_B. Experimentally, the measured differential reaction cross section refers frequently only to that leading to one of these J_B levels (usually, the sharpest level with $J_B = I + S$). In our investigation where a purely central nucleon-nucleon potential is assumed, the results obtained represent, however, the totality of differential reaction cross sections for the excitation of all possible J_B levels. Therefore, a direct comparison between calculation and experiment will necessarily show that our calculated differential reaction cross sections are too large. To remedy this defect, one obviously needs to introduce into the resonating-group formulation a nucleon-nucleon potential with non-central components, a project which we are in fact contemplating to carry out in the future. At the present moment, however, we can still proceed to examine the quality of the calculated results by comparing directly with experimental data. The reason for this is that, because all the J_B levels have a common value of I, it is not unreasonable to expect that differential reaction cross sections leading to different J_B levels will differ mainly in magnitude, but not in their oscillatory behavior.

These two factors indicate that we should generally expect our calculated differential reaction cross-section curve to lie above the data points, but to have a reasonably correct oscillatory shape. As will be seen below, this expectation does turn out to be generally the case.

3.2. 6-NUCLEON SYSTEM

The reaction of interest in the 6-nucleon system is the $\alpha(d,p){}^5\mathrm{He}$ reaction. In Fig. 3, we show, together with the experimental data, [21] the differential reaction cross sections at a c.m. energy of $E_1 = 16.2$ MeV in the $d + \alpha$ incident channel. For this reaction, the over-estimation effect of factor (a) discussed in the preceding subsection is not significant, since the model space used in this system is already large enough. On the other hand, it is necessary to recognize that the measured differential reaction cross section represents the contribution only from the $J_B = 3/2$, negative-parity ground state of ${}^5\mathrm{He}$ with $(I,S) = (1,1/2)$. From a purely statistical viewpoint, one will come to the conclusion that the contribution from its partner state with $J_B = 1/2$ should add 50 % to the measured value. However, we do not think that this latter contribution can be so large, simply because the $1/2^-$ state of ${}^5\mathrm{He}$ is a broad state with a very short lifetime. Thus, the over-estimation effect due to factor (b) of §3.1 is likly to be not too important, and a direct comparison between calculation and experiment should lead to a resonably favorable outcome.

The quality of the comparison shown in Fig. 3 is indeed quite satisfactory. It is not possible to assess the degree of over-estimation caused by factor (b) for the

obvious reason that the uncertainties associated with the data points are too large. The only conclusion that one can make is that the $\alpha(d,p)^5$He $(1/2^-)$ differential reaction cross section is most likely to be appreciably smaller than 50% of the corresponding cross section for the reaction $\alpha(d,p)^5$He $(3/2^-)$.

3.3. 7-NUCLEON SYSTEM

There is a number of interesting reactions in this system. Some of these are initiated from the ^{3}He + α channel, while the others are from the $n + ^6$Li channel. In the following, we shall discuss these reactions individually.

3.3.1. Reactions initiated from the ^{3}He + α channel

In Fig. 4, we show the $\alpha(^3\mathrm{He},p)^6$Li differential reaction cross sections at a c.m. energy of $E_1 = 15.95$ MeV in the ^{3}He + α incident channel. Experimental data shown are those of Ref. 14). Since in this case the partial reaction cross section at this energy is equal to only a small part (i.e., 14%) of the ^{3}He + α total reaction cross section, we expect that to achieve a detailed explanation of the experimental data will not be a simple task. In fact, one sees from this figure that the comparison between calculation and experiment is only fair. The calculation yields a reasonable oscillatory pattern and rather satisfactory general magnitudes, but there is no detailed agreement. The most obvious discrepancy seems to be that the oscillation amplitudes of the calculated curve are too large. However, this should not be considered as a serious defect, since it can be easily remedied by including noncentral forces in the calculation. On the other hand, this discrepancy does have the unfortunate consequence of making it difficult to discern the over-estimation effect caused by factor (a). The only reasonable conclusion that could be made from the comparison shown in Fig. 4 is that this effect is not likely to be very large, which is consistent with the fact that the calculated ^{3}He + α total reaction cross section is only about 30 % smaller than the measured value (see Table II).

The $\alpha(^3\mathrm{He},p)^6\mathrm{Li}^*$ partial reaction cross section constitutes also only a rather minor part, equal to about 26 %, of the ^{3}He + α total reaction cross section at $E_1 = 15.95$ MeV. As a consequence, the quality of comparison between calculated and experimental [14] differential cross sections for this reaction, shown in Fig. 5, is similar to that in the $\alpha(^3\mathrm{He},p)^6$Li case. There is one point that we should mention, however; that is, the over-estimation effect caused by factor (b) must also be considered, since the measured result represents only the contribution from the 2.18-MeV, 3^+ excited state of ^{6}Li with $(I,S) = (2,1)$. Unfortunately, we find that, here again, the large oscillation amplitudes of the calculated curve preclude a clear assessment of the significance of this effect. Therfore, we are compelled to conclude that even though the present large-model-space calculation is extensive enough to achieve a general understanding of the essential features in the 7-nucleon system, a detailed comparison with experiment can be made only after we make the generalization to include noncentral and Coulomb forces in the formulation.

Calculated differential cross sections for the reaction $\alpha(^3\mathrm{He},d)^5$Li at $E_1 = 15.95$ MeV are shown in Fig. 6. No data points are shown, since we are not aware of the existence of any such data at this time. We choose to show the calculated results here, simply because this reaction is the dominant one among reactions initiated from the ^{3}He + α incident channel, and contributes to around 60 % of the ^{3}He + α total reaction cross section at 15.95 MeV. It proceeds by a one-nucleon transfer process, with the consequence of producing large differential reaction cross sections in the forward angular region (see the discussion given in Ref. 2)). Clearly, an experimental determination of these cross sections would undoubtedly be desirable, since it can certainly yield information that adds further to our present understanding about the basic mechanisms occurring in nuclear reactions.

3.3.2. Reactions initiated from the $n + ^6$Li channel

We consider first the inelastic-scattering reaction $^6\mathrm{Li}(n,n')^6\mathrm{Li}^*$. In this case, there is a favorable factor which tends to lessen the undesirable feature of excessive

oscillation amplitudes in the cross sections caused by the omission of noncentral forces in the calculation. This factor is that the calculated differential reaction cross section consists of incoherent contributions from both the $S = 3/2$ and the $S = 1/2$ channels. Such an incoherent addition will usually have the net effect of smoothing out the peaks and valleys in the cross-section curve (see Fig. 3 of Ref. 22) for an explicit demonstration of this smoothing effect), and thereby facilitates the comparison between calculation and experiment.

A comparison between calculated and experimental [15] differential cross sections for the ^{6}Li$(n,n')^6$Li* reaction at c.m. energies of $E_2 = 8.57$ and 12 MeV in the $n + ^6$Li channel is shown in Fig. 7. Here one sees that the calculation reproduces nicely the rather structureless behavior of the data points. The calculated magnitudes are too large by a factor of about 2, which is a discrepancy arising from the over-estimation effect caused by factors (a) and (b) discussed in §3.1. To gain some idea about the effect of factor (a), we can make an examination of the $n + ^6$Li elastic-scattering case, because its differential cross section is similarly affected by this particular factor. From the comparison shown in Fig. 14 of Ref. 5), we note that the over-estimate is in fact rather modest, being only around 20 %. This is, of course, a reflection of the finding, shown in Table II, that the calculated $n + ^6$Li total reaction cross sections at these energies are already equal to about 80 % of the measured values. In contrast to this, the over-estimation effect caused by factor (b), relating to the fact that the experimental cross section represents only the contribution from the 2.18-MeV, 3^+ excited state of ^{6}Li, is likely to be considerably more important. From purely statistical viewpoints, one expects that the differential cross sections for the reactions ^{6}Li$(n,n')^6$Li$^*(2^+)$ and ^{6}Li$(n,n')^6$Li$^*(1^+)$ should be equal to 5/7 and 3/7 of the ^{6}Li$(n,n')^6$Li$^*(3^+)$ cross section, respectively. In practice, because of the short lifetimes of the 2^+ and 1^+ states, their contributions would probably be appreciably smaller. Even so, one can still reasonably conclude by using these qualitative arguments that the combined effect of factors (a) and (b) may very conceivably explain the discrepancy observed here for the comparison between calculated and experimental results.

Next, we show in Fig. 8 the calculated differential cross sections for the reaction ^{6}Li$(n,d)^5$He at $E_2 = 12$ MeV. Experimental data shown are those of Higuchi *et al.*[23] (see also Table 1 of Ref. 24)) and Volković *et al.*[25] for contributions leading to the $3/2^-$ ground state of ^{5}He. As is seen from this figure, the calculated curve does exhibit a correct behavior, with a significant rise in the backward angular region. The calculated magnitudes are again somewhat too large, although the cross-section over-estimate is not as substantial as that in the ^{6}Li$(n,n')^6$Li* case described in the preceding paragraph. This latter observation can be qualitatively understood by invoking the statistical arguments that have been discussed above for the situations where ^{5}He and ^{6}Li* are the nuclear entities in the exit channels. The major discrepancy seems to occur at extreme forward angles where the calculated curve shows a prominent dip, while the data points show a flat behavior. We believe that this is an undesirable feature which arises again from the omission of noncentral and Coulomb forces in the formulation and should certainly be carefully looked into in the future when more powerful computational facilities become readily available.

A comparison between calculated and experimental differential cross sections for the reaction ^{6}Li$(n,t)\alpha$ at $E_2 = 12$ MeV is depicted in Fig. 9. The experimental data shown are those of Higuchi *et al.*[23] (see also Table 1 of Ref. 24)), Volković *et al.*, [26] and Rendić and Paić. [27] Since this reaction is just the inverse of the reaction $\alpha(t,n)^6$Li, all the discussion given in §3.3.1 for the $\alpha(^3$He$,p)^6$Li reaction is also applicable here. The smoothing effect described above is no longer in operation, because the reaction proceeds only through a single $S = 1/2$ channel. As a result of this, the overestimation effect, caused by factor (a) which is not expected to be very large in any case, cannot be discerned from the comparison shown in this figure.

3.4. 8-NUCLEON SYSTEM

The cases to be discussed are the elastic-scattering process $n+^7$Li, the inelastic-scattering reaction $^7\mathrm{Li}(n,n')^7\mathrm{Li}^*$, and the rearrangement reaction $^7\mathrm{Li}(n,t)^5\mathrm{He}$. We discuss $n+^7$Li scattering here, simply because our results described previously in Ref. 6) contains a phase error in the computation, and it is necessary to present the corrected results.

In Fig. 10, we compare the calculated and experimental [15] differential cross sections for $n+^7$Li scattering at c.m. energies of $E_1 = 9.58$ and 12.2 MeV. Here one sees that the quality of fit is similar to that in the $n+^6$Li case shown in Fig. 14 of Ref. 5). The calculation reproduces quite well the oscillatory features of the measured results. The only notable discrepancy seems to occur at backward angles beyond 140°, which is most likely due to the fact that certain cluster configurations may still need to be included in the calculation. The over-estimate caused by factor (a), as determined by comparing the calculated and experimental cross sections at the peaks near 110°, is around 15 %. This is consistent with the finding that the calculated $n+^7$Li total reaction cross sections are already fairly reasonable, being equal to about 75 % of the experimental values (see Table II).

For the next case, we consider the inelastic-scattering reaction $^7\mathrm{Li}(n,n')^7\mathrm{Li}^*$ at $E_1 = 10.54$ and 12.2 MeV. In Fig. 11, calculated differential reaction cross sections are shown, together with the experimental data. [15] Here it is seen that the rather structureless behavior of the angular distributions is very well reproduced. For this reaction, there exist over-estimation effects arising from both factors (a) and (b), because the experimental values represent only the inelastic contributions from the 4.63 - MeV, $7/2^-$ excited state of ^{7}Li with $(I,S) = (3,1/2)$. As has been discussed above, the over-estimate in the calculated cross section due to factor (a) is only of moderate importance. Regarding factor (b), we note that, based on purely statistical arguments, the $^7\mathrm{Li}(n,n')^7\mathrm{Li}^*(5/2^-)$ cross section is equal to 3/4 of the $^7\mathrm{Li}(n,n')^7\mathrm{Li}^*(7/2^-)$ cross section. However, because of the short lifetime of the $5/2^-$ excited state, the actual contribution from this state may not be nearly so

significant. Therefore, with both of these two factors taken into account, one can reasonably make the statement that the over-estimate of about 30 - 40 % in the calculated differential reaction cross section at 12.2 MeV is not at all surprising.

What is not expected is that there is a good agreement between calculated and experimental $^7\mathrm{Li}(n,n')^7\mathrm{Li}^*$ differential reaction cross sections at 10.54 MeV. The over-estimation effects, shown above to be moderately significant, do not seem to be present at this lower energy. We think, however, that this surprisingly good result is somewhat fortuitous, and the reason for its occurrence may be as follows. Because of the complicated nature of a many-nucleon system, one expects that even a rather extensive multiconfiguration RGM study will not be able to precisely yield the positions of compound-nucleus resonances and energy thresholds. As a consequence, it would generally be prudent to avoid the low-energy region and examine the results only in a higher-energy region which is not too close to sharp resonances and the thresholds of the various cluster configurations. In the present case, it is unfortunate that, for $E_1 = 10.54$ MeV, this precautionary criterion is not too well satisfied (see Figs. 3 and 15 of Ref. 6)). Thus, the calculated magnitudes of the differential reaction cross section at this energy may be somewhat less reliable than those at higher energies, and an accidental agreement with experiment ensues.

Calculated and experimental differential cross sections for the reaction $^7\mathrm{Li}(n,t)^5\mathrm{He}$ at $E_1 = 12.2$ MeV are compared in Fig. 12. In this case, there is the unfortunate situation that the data of Shirato *et al.*[24] and Volković *et al.*[26,28] do not seem to be consistent with each other. As a result, the only statement that can be made is that there is no obvious discrepancy between calculated and experimental results. At the present moment, it is not even possible to estimate the significance of the over-estimation effects, because of the poor quality of the existing data. Quite clearly, more accurate experimental measurements should be made in order to enable us to come up with more definitive conclusions.

3.5. 10-NUCLEON SYSTEM

In the 10-nucleon system, we have studied the $\alpha+{}^6\mathrm{Li}$ elastic-scattering process, the ${}^6\mathrm{Li}(\alpha,d){}^8\mathrm{Be}$ rearrangement process, and the ${}^6\mathrm{Li}(\alpha,\alpha'){}^6\mathrm{Li}^*$ inelastic-scattering process. For the former two processes, the results have already been presented in a previous publication, [9] but will be further discussed here for additional information regarding the adequacy of the chosen model space which is specified in the last row of Table I.

Comparisons of calculated and experimental differential cross sections for $\alpha+{}^6\mathrm{Li}$ scattering at $E_1 = 27$ MeV and ${}^6\mathrm{Li}(\alpha,d){}^8\mathrm{Be}$ reaction at $E_1 = 12$ MeV are shown in Figs. 3 and 4 of Ref. 9), respectively. From these figures, one finds that the calculation again reproduces rather well the general features of the measured angular distributions, such as the cross-section rise at backward angles and the angular positions of peaks and valleys. However, the calculated magnitudes of the differential cross sections are too large by a factor of about 2 in both cases. This indicates that the over-estimation effect, caused by factor (a), is appreciably more important in the 10-nucleon calculation than in the 6-, 7- and 8-nucleon calculations. In turn, this would suggest that the value of 0.71 for the ratio ρ, given in Table II, is quite likely an over-estimate. We think that this is a reasonable suggestion, because the calculated $\alpha+{}^6\mathrm{Li}$ total reaction cross section is not directly compared with the measured value, which is not available at the present moment, but is compared with an empirical value [19] obtained from a single-configuration $\alpha+{}^6\mathrm{Li}$ resonating-group study supplemented by a phenomenological imaginary potential to approximately account for reaction effects. Apparently, such an indirect way to estimate the $\alpha+{}^6\mathrm{Li}$ total reaction cross section is simply too crude to yield a result which is sufficiently reliable. Based on our observation here, it is quite clear that, to gauge the adequacy of the 10-nucleon model space used in our present calculation, one will need to have experimental values for the total reaction cross section, which are as accurate as those available in the 6-, 7- and 8-nucleon systems.

For the ${}^6\mathrm{Li}(\alpha,\alpha'){}^6\mathrm{Li}^*$ reaction, the over-estimation effect caused by factor (b) must also be considered, since the experimental results represent only contributions from the 3^+, first excited state of ${}^6\mathrm{Li}$. To estimate the importance of this effect, we make use of the experience learned from the ${}^6\mathrm{Li}(n,n'){}^6\mathrm{Li}^*$ calculation (see §3.3.2) where it is found that the over-estimate in the differential reaction cross section due to factor (b) is around 80 % or so. Thus, with both factors (a) and (b) taken into account, we expect that the calculated ${}^6\mathrm{Li}(\alpha,\alpha'){}^6\mathrm{Li}^*$ differential reaction cross section can be as large as about 4 times the measured value. That this turns out to be indeed the case can be seen from Fig. 13, where the calculated cross sections are compared with the experimental results obtained by Bernas *et al.* at 20.85 and 27 MeV. [29] Here it is seen that, inspite of the large difference in magnitudes, the calculated curve do exhibit the general behavior of the data points. This is clearly an encouraging finding, and suggests that it will certainly be worthwhile to improve the calculation by enlarging the model space and by including noncentral and Coulomb forces in the formulation.

4. Conclusion

Differential cross sections for various reactions in the 6-, 7-, 8- and 10-nucleon systems, obtained by using multiconfiguration RGM calculations, are compared with experimental results. These comparisons show that the calculation can satisfactorily explain the general features of the measured angular distributions, such as the cross-section rise at backward angles, the angular positions of cross-section maxima and minima, and so on. The only undesirable finding is that the calculated magnitudes are somewhat too large, but this can be qualitatively understood as resulting from the various simplifications adopted in the calculation. These simplifications must of course be relinquished if one desires to obtain a detailed and quantitative agreement with experiment. This can be accomplished by further expanding the model space and by adopting a more realistic nucleon-nucleon potential. For example, in the 10-nucleon case, it will be desirable to introduce

noncentral and Coulomb forces, and use a 4-cluster $\alpha+\alpha+n+p$ formulation such that the ^{5}He + ^{5}Li, n + ^{9}B and p + ^{9}Be cluster configurations can also be taken into consideration. Quite clearly, these improvements can be straightforwardly incorporated but, unfortunately, will require a great deal of computational effort. At the present moment, we have already completed all the necessary analytical work, [30] and are prepared to start the numerical phase as soon as more advanced computational facilities become readily accessible.

Together with our previous discussions on level spectra and scattering cross sections,[3,5 -9] this investigation shows quite convincingly that the RGM, being a sound microscopic method built on firm physical foundation, can be used to treat nuclear bound-state, scattering, and reation problems in a unified and consistent manner. At present, this method has mainly been applied to relatively light systems, because of complexities in analytical derivations and limitations in computational capabilities. However, with reasonable simplifications achieved through understanding in reaction mechanisms and nucleon-exchange contributions, [2] there is no doubt in our mind that this method can eventually be used to achieve a unified and fundamental understanding of all the interesting and intricate phenomena exhibited by even medium- and heavy-weight nuclear systems.

Acknowledgements

We would like to acknowledge the generous grant of computer time by the Research Center for Nuclear Physics at the Osaka University and by the Supercomputer Institute at the University of Minnesota.

REFERENCES

1. K. Wildermuth and Y. C. Tang, *A Unified Theory of the Nucleus, Clustering Phenomena in Nuclei*, Vol. 1, ed. K. Wildermuth and P. Kramer (Vieweg, Braunschweig, Germany, 1977).
2. Y. Fujiwara and Y. C. Tang, Prog. Theor. Phys. **91** (1994), 631, and references contained therein.
3. Y. Fujiwara and Y. C. Tang, Few Body Systems **12** (1992), 21.
4. B. Jenny, W. Grüebler, V. König, P. A. Schmelzbach and C. Schweizer, Nucl. Phys. **A397** (1983), 61.
5. Y. Fujiwara and Y. C. Tang, Nucl. Phys. **A522** (1991), 459.
6. Y. Fujiwara and Y. C. Tang, Phys. Rev. **C41** (1990), 28.
7. Y. Fujiwara and Y. C. Tang, Few Body Systems **16** (1994), 91.
8. Y. Fujiwara and Y. C. Tang, Phys. Rev. **C43** (1991), 96.
9. Y. Fujiwara and Y. C. Tang, submitted to Prog. Theor. Phys.
10. H. Kanada, T. Kaneko and Y. C. Tang, Phys. Rev. **C43** (1991), 371; Nucl. Phys. **A504** (1989), 529.
11. K. Langanke, Adv. Nucl. Phys. **21** (1994), 85, and references given therein.
12. H. M. Hofmann, T. Mertelmeier and W. Zahn, Nucl. Phys. **A410** (1983), 208.
13. D. R. Thompson, M. LeMere and Y. C. Tang, Nucl. Phys. **A286** (1977), 53.
14. J. A. Koepke and R. E. Brown, Phys. Rev. **C16** (1977), 18.
15. H. H. Hogue, P. L. von Behren, D. W. Glasgow, S. G. Glendinning, P. W. Lisowski, C. E. Nelson, F. O. Purser, W. Tornow, C. R. Gould and L. W. Seagondollar, Nucl. Sci. Eng. **69** (1979), 22.
16. J. A. Cookson, D. Dandy and J. C. Hopkins, Nucl. Phys. **A91** (1967), 273.

17. D. W. Kneff, B. M. Oliver, E. Goldberg and R. C. Haight, Nucl. Sci. Eng. **94** (1986), 136.

18. D. G. Foster, Jr. and D. W. Glasgow, Phys. Rev. **C3** (1971), 576.

19. M. LeMere, Y. C. Tang and H. Kanada, Phys. Rev. **C25** (1982), 2902.

20. Y. C. Tang and R. E. Brown, Phys. Rev. **C4** (1971), 1979.

21. H. J. Erramuspe and R. J. Slobodrian, Nucl. Phys. **49** (1963), 65.

22. D. J. Stubeda, M. LeMere and Y. C. Tang, Phys. Rev. **C17** (1978), 447.

23. S. Higuchi, K. Shibata, S. Shirato and H. Yamada, Nucl. Phys. **A384** (1982), 51.

24. S. Shirato, S. Shibuya, K. Hata, Y. Ando and K. Shibata, Japan Atomic Energy Research Institute report JAERI-M 89-107 (1989).

25. V. Valković, G. Paić, I. Šlaus, P. Tomaš, M. Cerineo and G. R. Satchler, Phys. Rev. **139B** (1965), 331.

26. V. Valković, I. Šlaus, P. Tomaš and M. Cerineo, Nucl. Phys. **A98** (1967), 305.

27. D. Rendić and G. Paić, Rossendorf Reports **2** (1967), 143.

28. D. Miljanić, M. Furić and V. Valković, Nucl. Phys. **A148** (1970), 312.

29. M. Bernas, R. DeVries, B. G. Harvey, D. Hendrie, J. Mahoney, J. Sherman, J. Steyaert and M. S. Zisman, Nucl. Phys. **A242** (1975), 149.

30. Y. Fujiwara and Y. C. Tang, "Multicluster Resonating-Group Method of s-Shell Cluster Systems", Memoirs of the Faculty of Science, Kyoto University, Series A of Physics, Astrophysics, Geophysics and Chemistry, Vol. XXXIX, No. 1, Article 5 (1994), 91.

Tables

Table I. Model spaces used in the 6-, 7-, 8- and 10-nucleon systems and the values of the exchange-mixture parameter u.

nucleon number	3-cluster configuration	2-cluster configurations				u
		a	b	c	d	
6	$n+p+\alpha$	$d+\alpha$	$1N+5N$	PIC		0.98
7	$n+d+\alpha$	$t+\alpha$	$n+{}^6\mathrm{Li}$	$n+{}^6\mathrm{Li}^*$	$d+{}^5\mathrm{He}$	1.0
8	$n+t+\alpha$	$n+{}^7\mathrm{Li}$	$t+{}^5\mathrm{He}$	$n+{}^7\mathrm{Li}^*$	${}^4\mathrm{H}+\alpha$	1.0
10	$d+\alpha+\alpha$	$\alpha+{}^6\mathrm{Li}$	$d+{}^8\mathrm{Be}$	$d+{}^8\mathrm{Be}^*$	$\alpha+{}^6\mathrm{Li}^*$	0.907

Table II. Total reaction cross sections σ_R in various light nuclear systems. For the $\alpha+{}^6\mathrm{Li}$ system, an empirical value deduced in Ref. 19) is employed.

Incident channel	c.m. energy (MeV)	σ_R (mb)		ratio ρ	References for exp'tal σ_R
		Calc.	Exp't		
$d+\alpha$	10.0	470	510	0.92	4)
	22.0	294	309	0.95	
${}^3\mathrm{He}+\alpha$	15.95	296	426	0.7	14)
$n+{}^6\mathrm{Li}$	8.57	515	654	0.79	15), 16)
	12.8	423	512	0.83	17)
$n+{}^7\mathrm{Li}$	12.2	286	386	0.74	15), 18)
$\alpha+{}^6\mathrm{Li}$	27	579	816	0.71	19)

Figure captions

Fig. 1: Differential cross sections for $n + {}^7\mathrm{Li}$ scattering at 12.2 MeV, obtained with SC, DC2, TC and QC calculations.

Fig. 2: Differential cross sections for the reaction ${}^7\mathrm{Li}(n,n'){}^7\mathrm{Li}^*$ at 12.2 MeV, obtained with DC2, TC and QC calculations.

Fig. 3: Comparison of calculated and experimental differential cross sections for the reaction ${}^4\mathrm{He}(d,p){}^5\mathrm{He}$ at 16.2 MeV. Experimental data shown are those of Ref. 21).

Fig. 4: Comparison of calculated and experimental differential cross sections for the reaction ${}^4\mathrm{He}({}^3\mathrm{He},p){}^6\mathrm{Li}$ at 15.95 MeV. Experimental data shown are those of Ref. 14).

Fig. 5: Comparison of calculated and experimental differential cross sections for the reaction ${}^4\mathrm{He}({}^3\mathrm{He},p){}^6\mathrm{Li}^*$ at 15.95 MeV. Experimental data shown are those of Ref. 14).

Fig. 6: Calculated differential cross sections for the reaction ${}^4\mathrm{He}({}^3\mathrm{He},d){}^5\mathrm{Li}$ at 15.95 MeV.

Fig. 7: Comparison of calculated and experimental differential cross sections for the reaction ${}^6\mathrm{Li}(n,n'){}^6\mathrm{Li}^*$ at 8.57 and 12 MeV. Experimental data shown are those of Ref. 15).

Fig. 8: Comparison of calculated and experimental differential cross sections for the reaction ${}^6\mathrm{Li}(n,d){}^5\mathrm{He}$ at 12 MeV. Experimental data shown are those of Refs. 23 - 25).

Fig. 9: Comparison of calculated and experimental differential cross sections for the reaction ${}^6\mathrm{Li}(n,t){}^4\mathrm{He}$ at 12 MeV. Experimental data shown are those of Refs. 23), 24), 26) and 27).

Fig. 10: Comparison of calculated and experimental differential cross sections for $n + {}^7\mathrm{Li}$ scattering at 9.58 and 12.2 MeV. Experimental data shown are those of Ref. 15).

Fig. 11: Comparison of calculated and experimental differential cross sections for the reaction ${}^7\mathrm{Li}(n,n'){}^7\mathrm{Li}^*$ at 12.2 MeV. Experimental data shown are those of Ref. 15).

Fig. 12: Comparison of calculated and experimental differential cross sections for the reaction ${}^7\mathrm{Li}(n,t){}^5\mathrm{He}$ at 12.2 MeV. Experimental data shown are those of Refs. 24), 26) and 28).

Fig. 13: Comparison of calculated and experimental differential cross sections for the reaction ${}^6\mathrm{Li}(\alpha,\alpha'){}^6\mathrm{Li}^*$ at 20.85 and 27 MeV. Experimental data shown are those of Ref. 29).

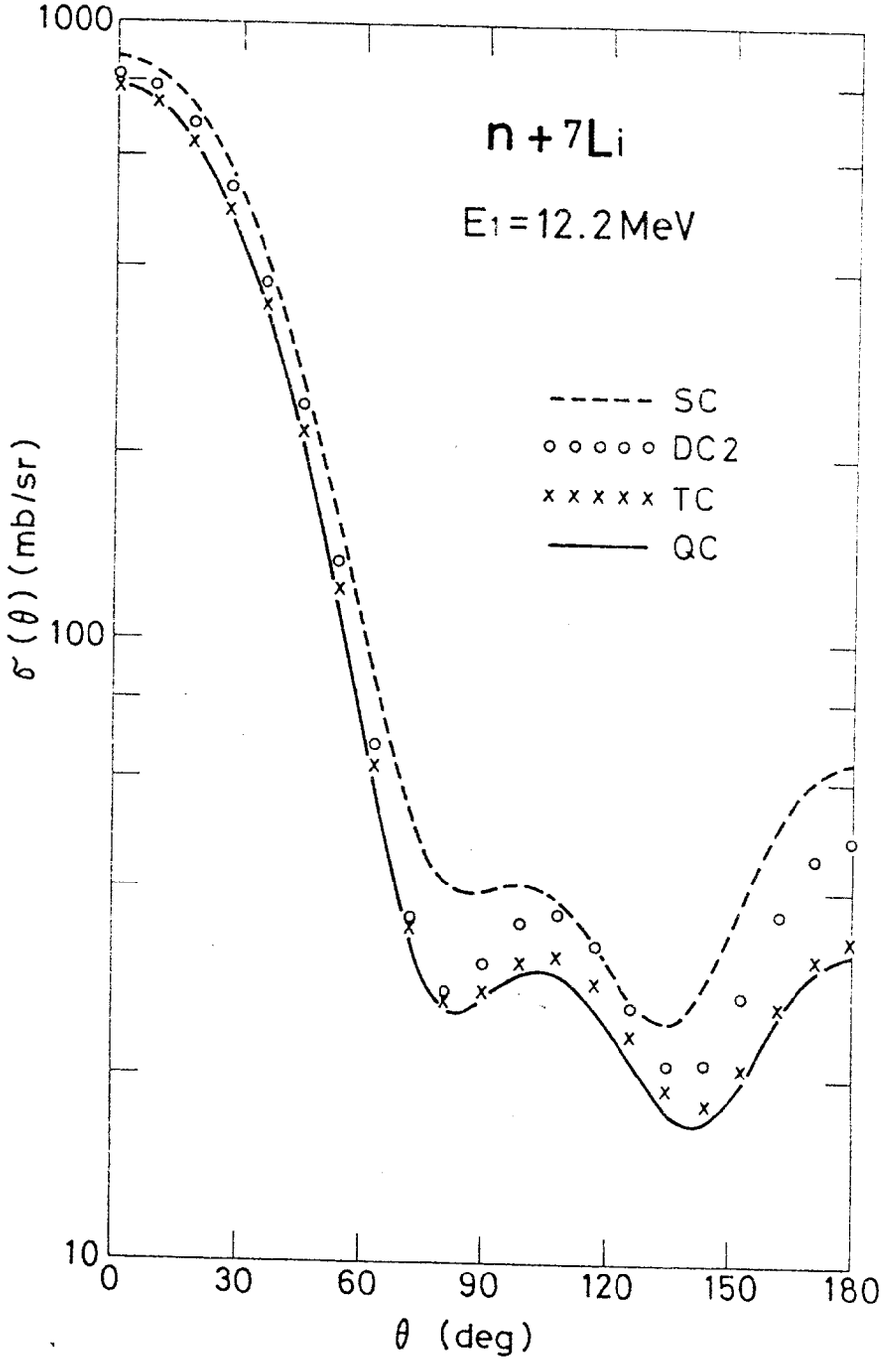
n + 7Li
E1 = 12.2 MeV
SC
DC2
TC
QC
σ (θ) (mb/sr)
θ (deg)
1000
100
10
0
30
60
90
120
150
180

Fig. 1

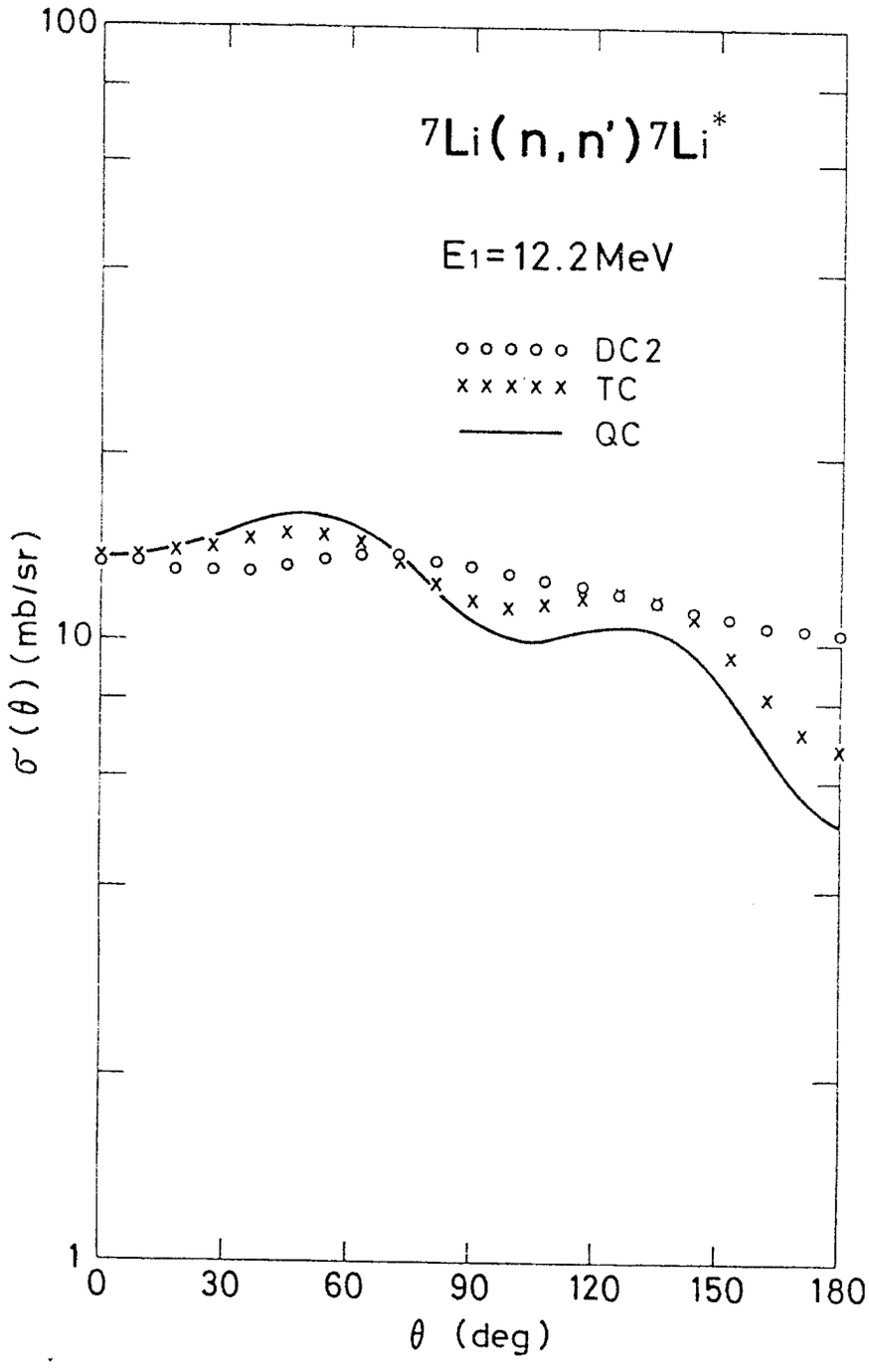
7Li (n, n') 7Li*
E1 = 12.2 MeV
DC2
TC
QC
σ (θ) (mb/sr)
θ (deg)
100
10
1
0
30
60
90
120
150
180

Fig. 2

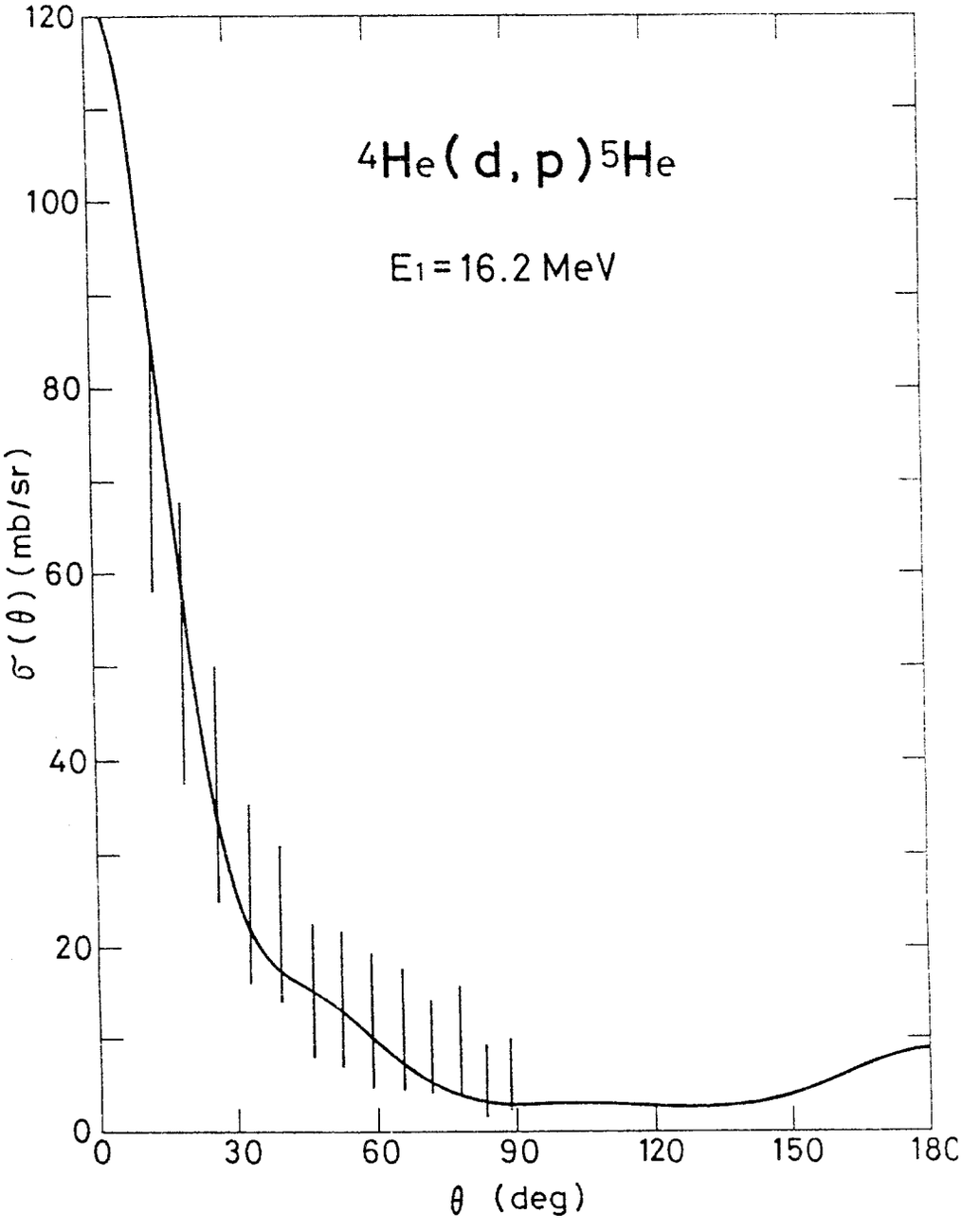
$^4He(d,p)^5He$
$E_1 = 16.2$ MeV
$\sigma(\theta)$ (mb/sr)
θ (deg)
0
20
40
60
80
100
120
0
30
60
90
120
150
180

Fig. 3

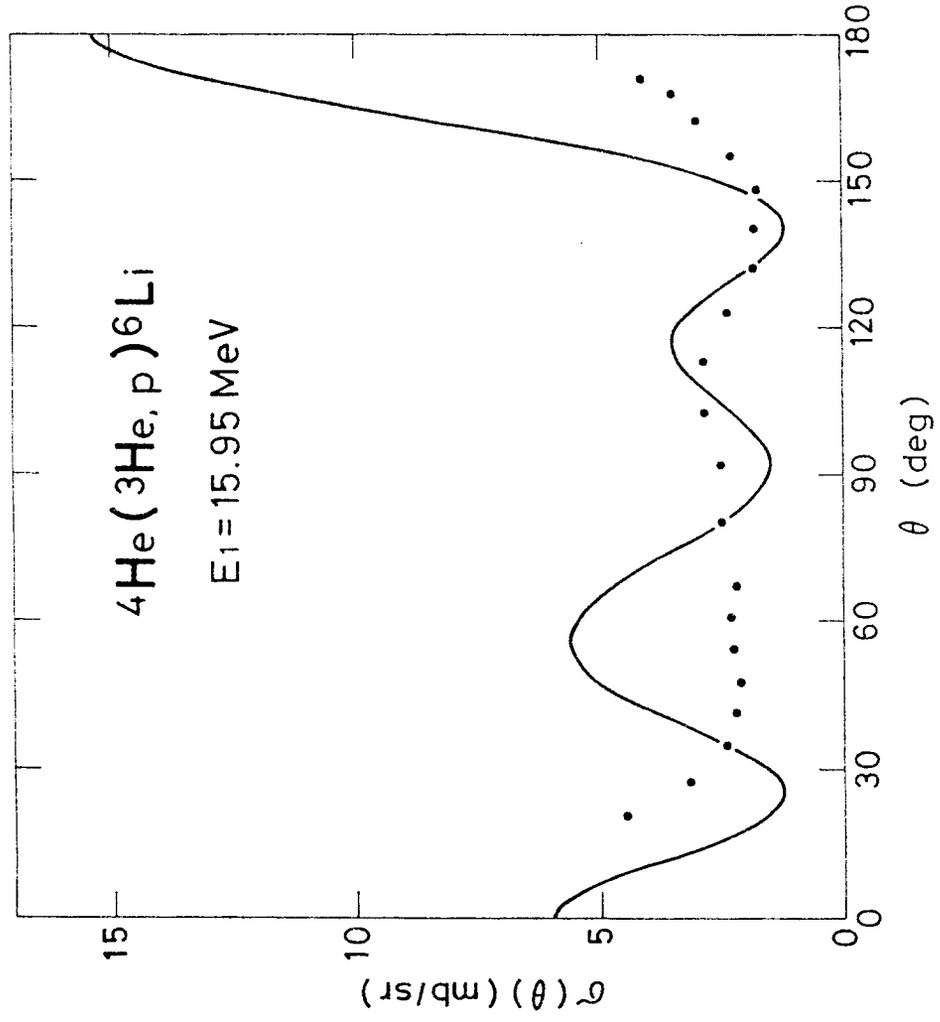
$^4He(^3He,p)^6Li$
$E_1 = 15.95$ MeV
$\sigma(\theta)$ (mb/sr)
θ (deg)
0
5
10
15
0
30
60
90
120
150
180

Fig. 4

Fig. 5

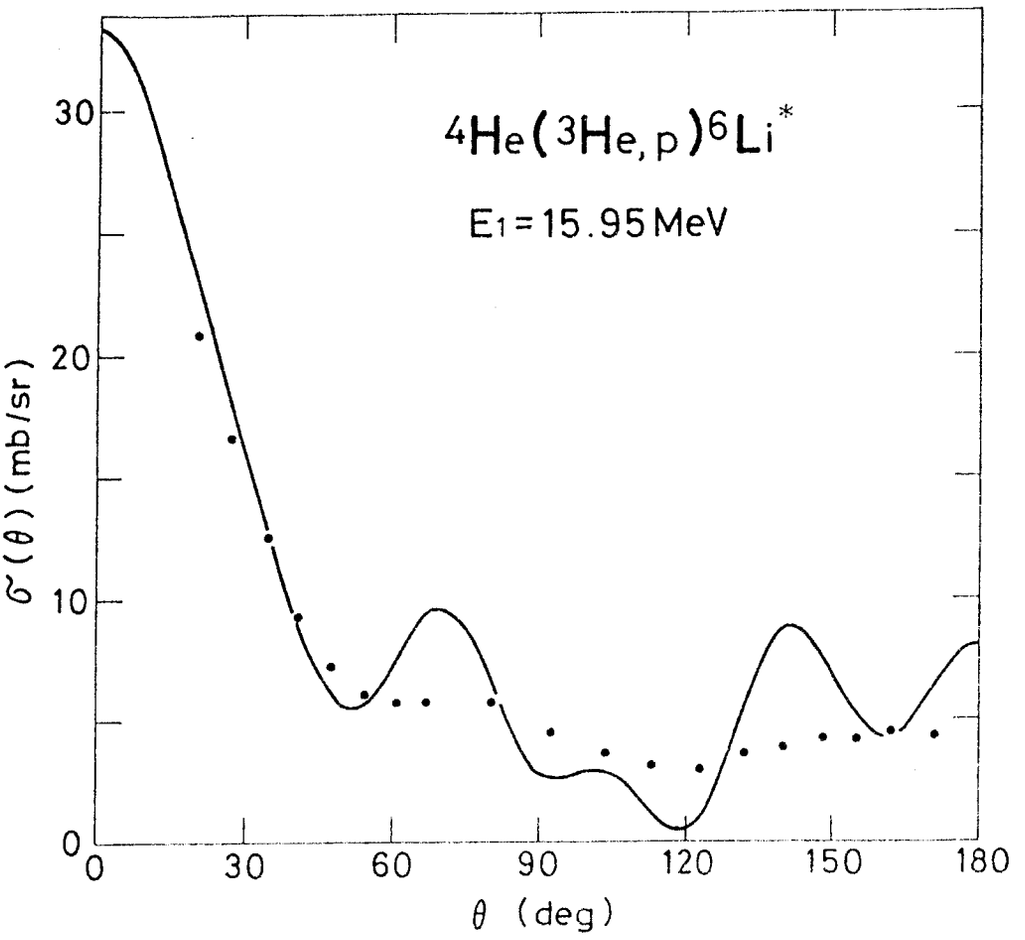
$^4He(^3He,p)^6Li^*$
$E_1 = 15.95$ MeV
$\sigma(\theta)$ (mb/sr)
θ (deg)
0
10
20
30
0
30
60
90
120
150
180

Fig. 6

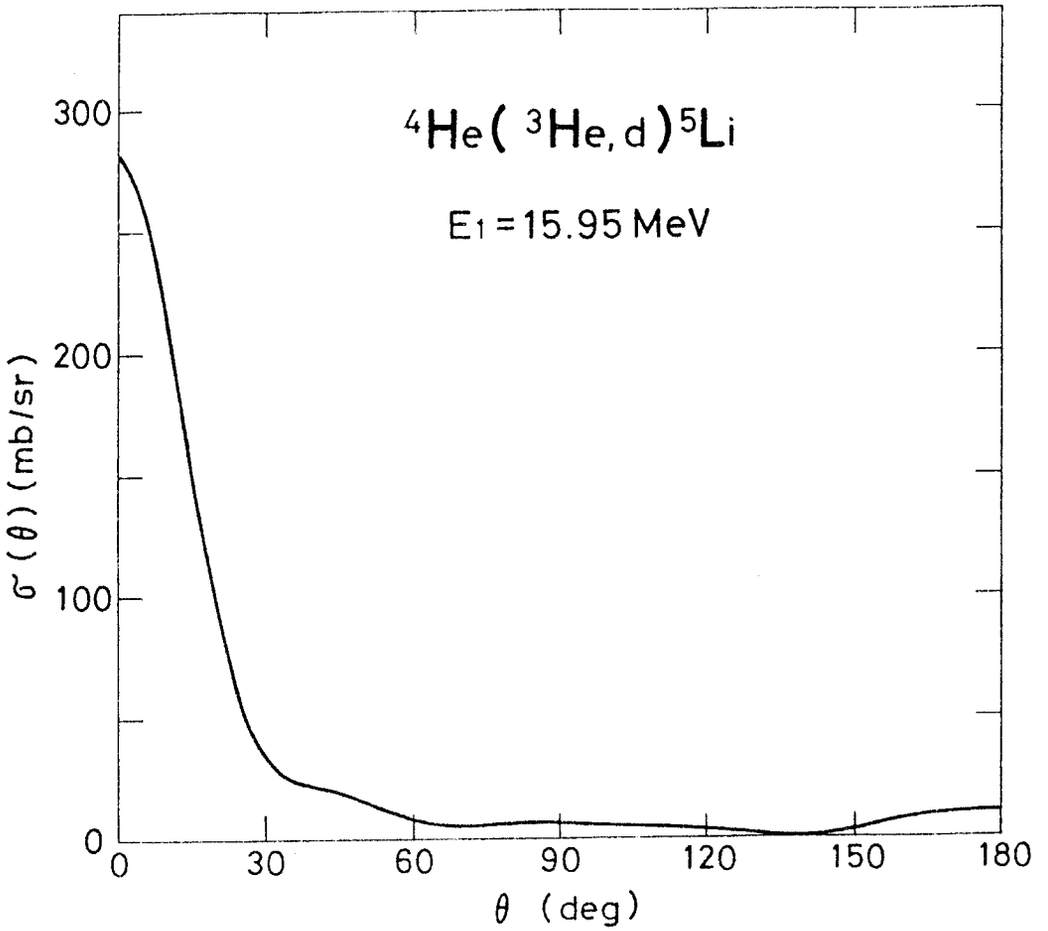
$^4He(^3He,d)^5Li$
$E_1 = 15.95$ MeV
$\sigma(\theta)$ (mb/sr)
θ (deg)
0
100
200
300
0
30
60
90
120
150
180

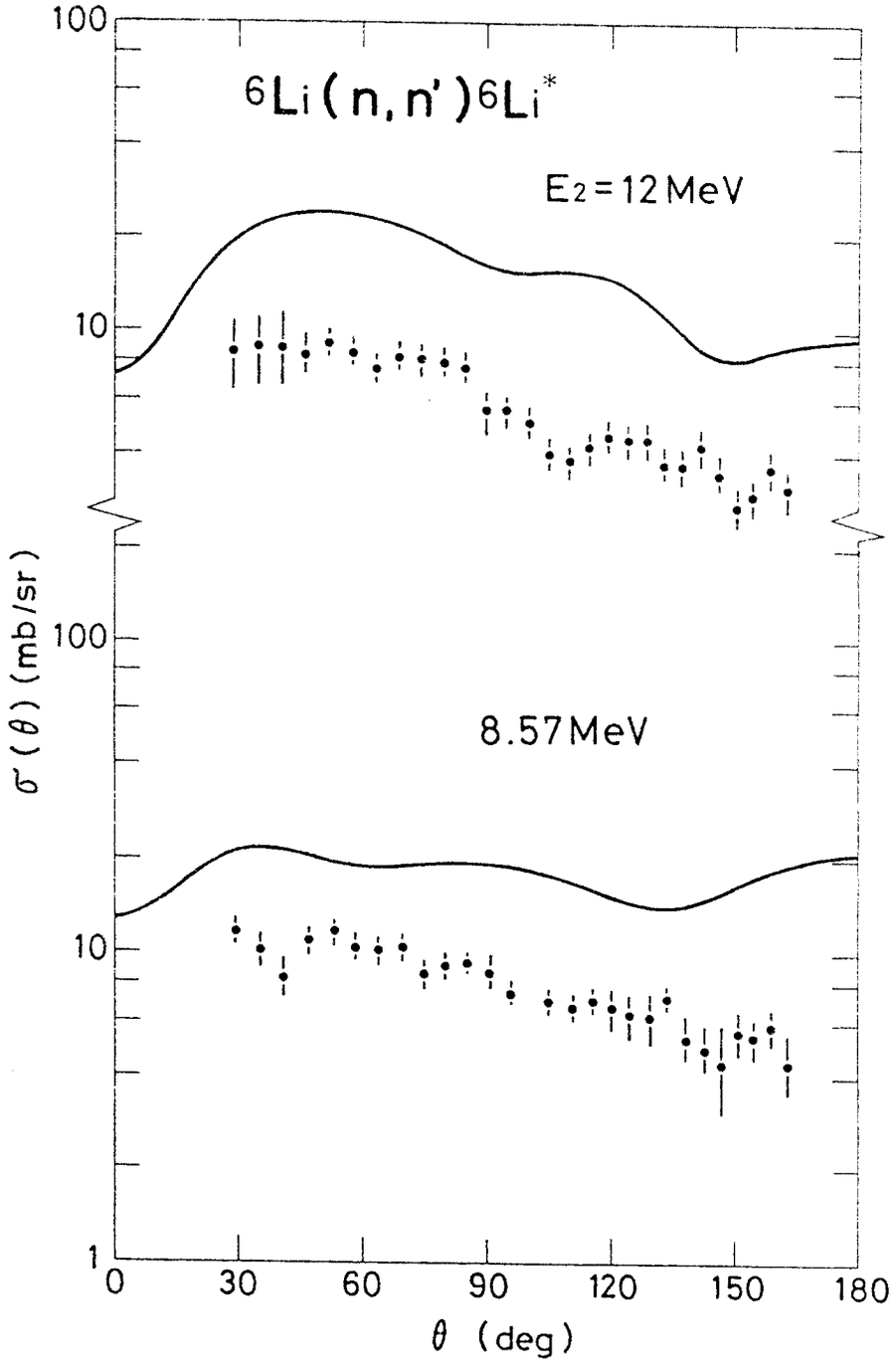
^{6}Li(n,n')^{6}Li*
E2=12MeV
8.57MeV
σ(θ) (mb/sr)
θ (deg)
100
10
1
100
10
0
30
60
90
120
150
180

Fig. 7

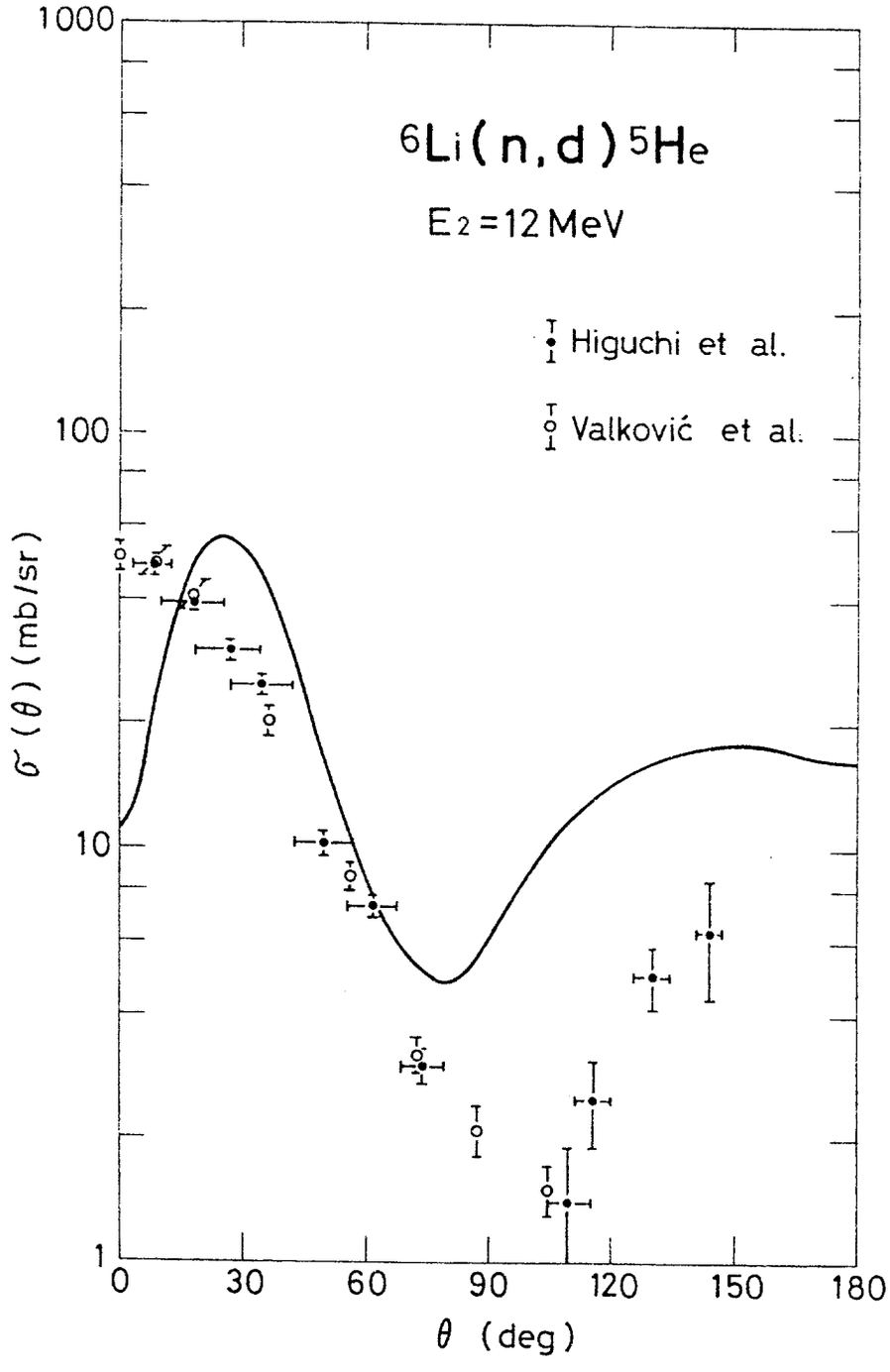
^{6}Li(n,d)^{5}He
E2=12MeV
Higuchi et al.
Valković et al.
σ(θ) (mb/sr)
θ (deg)
1000
100
10
1
0
30
60
90
120
150
180

Fig. 8

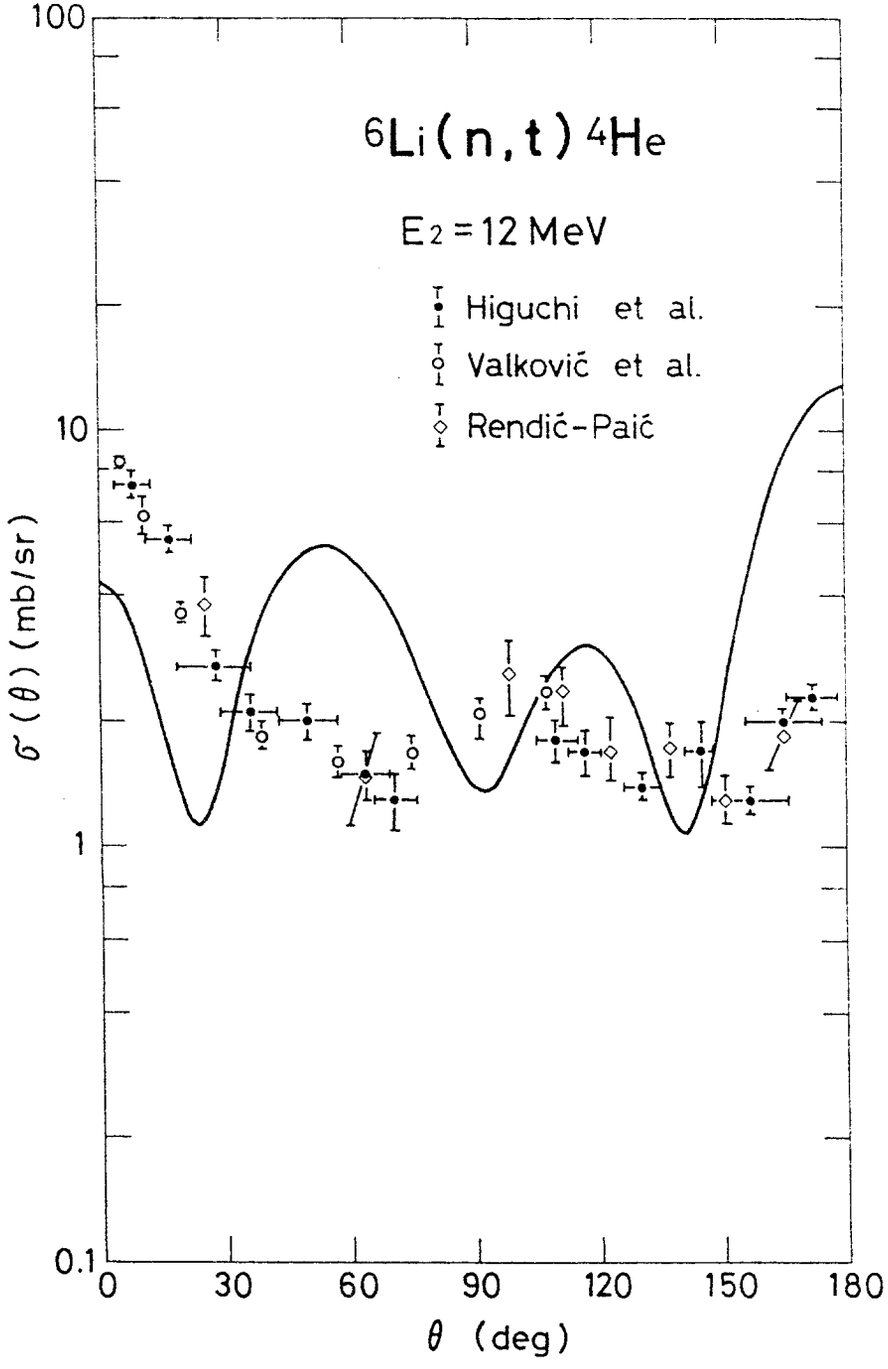
^{6}Li(n,t)^{4}He
E2 = 12 MeV
Higuchi et al.
Valković et al.
Rendić-Paić
σ(θ) (mb/sr)
θ (deg)
100
10
1
0.1
0
30
60
90
120
150
180

Fig. 9

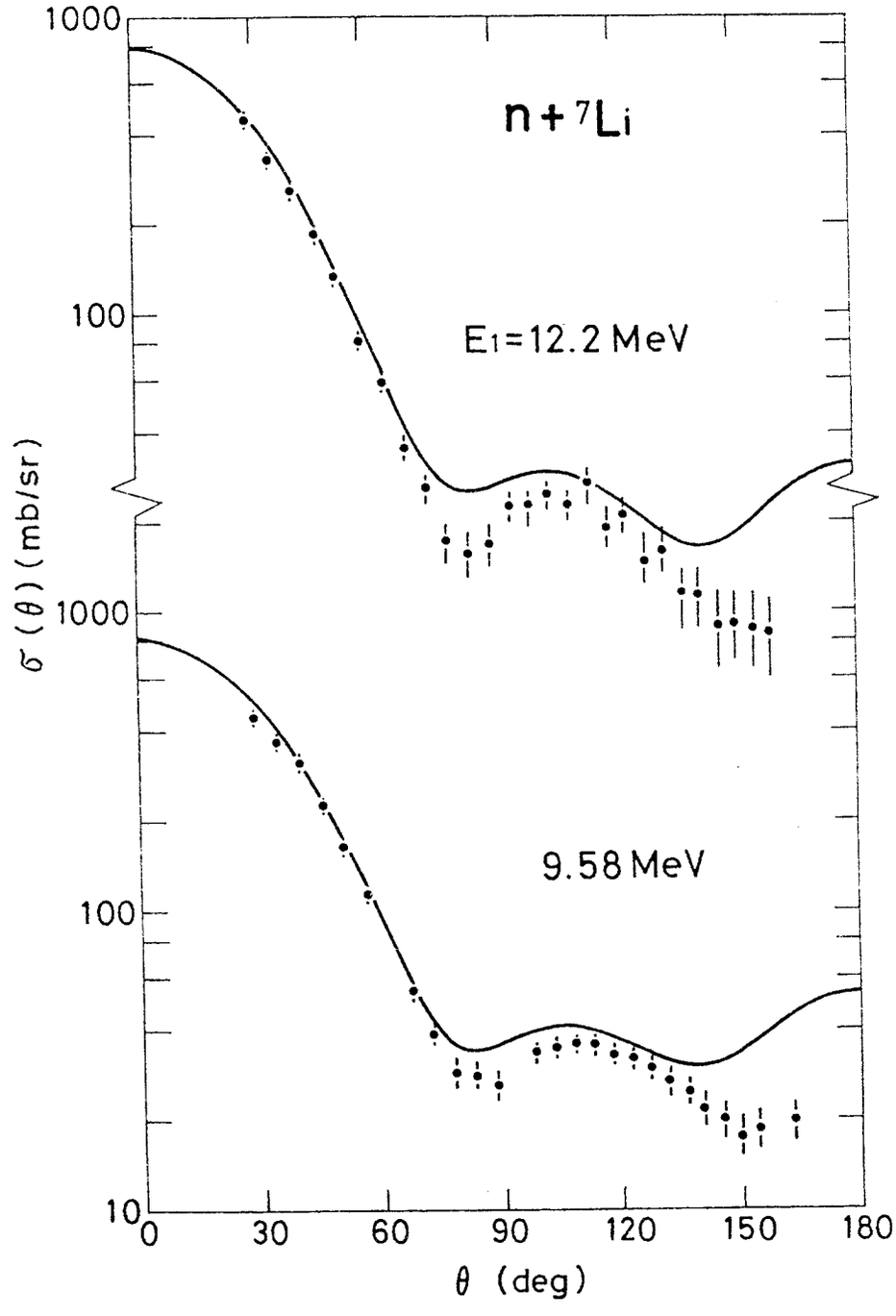
n + ^{7}Li
E1 = 12.2 MeV
9.58 MeV
σ(θ) (mb/sr)
θ (deg)
1000
100
1000
100
10
0
30
60
90
120
150
180

Fig. 10

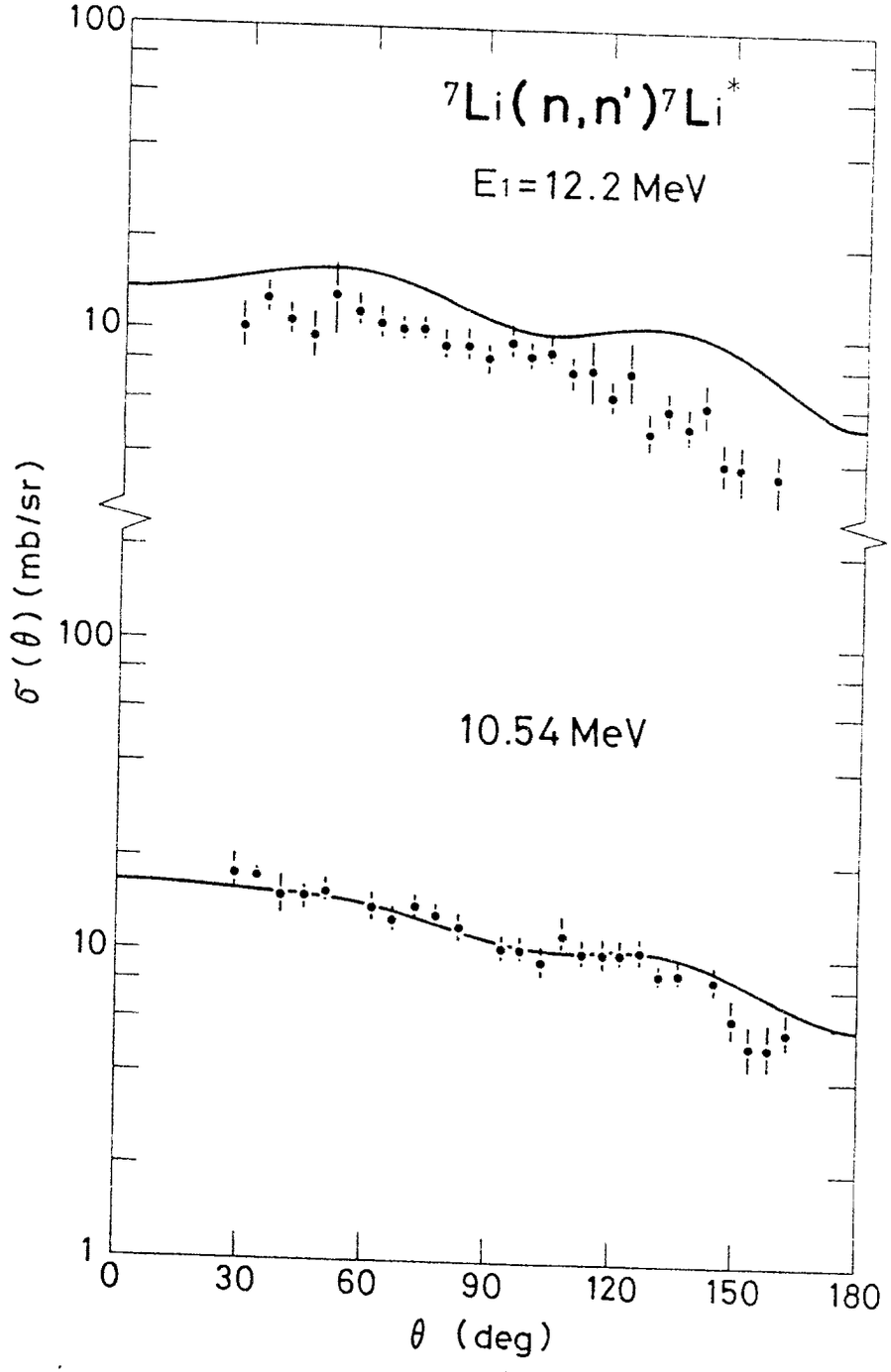
$^{7}Li(n,n')^{7}Li^{*}$
$E_1 = 12.2$ MeV
10.54 MeV
$\sigma(\theta)$ (mb/sr)
100
10
100
10
1
0
30
60
90
120
150
180
θ (deg)

Fig. 11

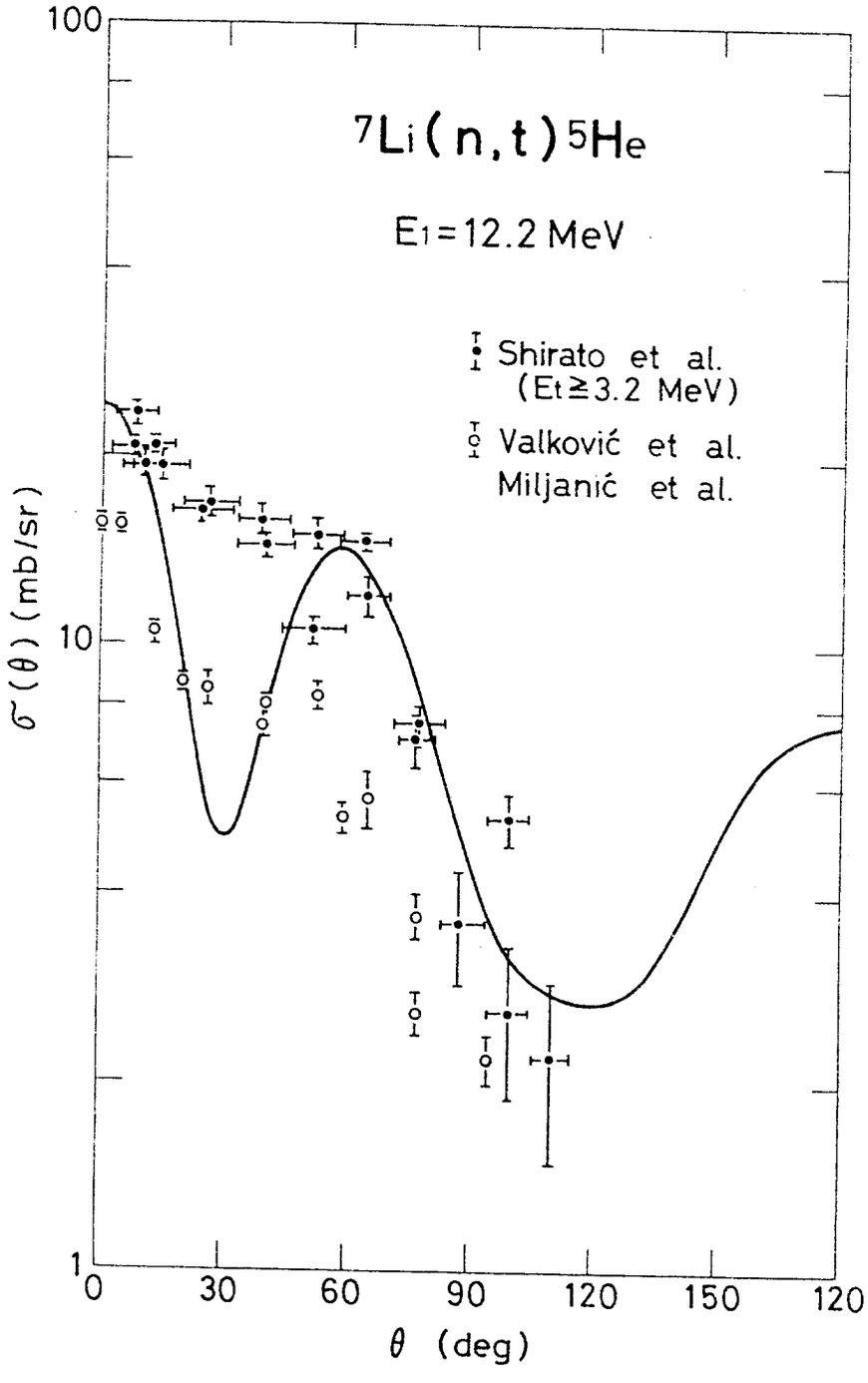
$^{7}Li(n,t)^{5}He$
$E_1 = 12.2$ MeV
Shirato et al.
($E_t \geq 3.2$ MeV)
Valković et al.
Miljanić et al.
$\sigma(\theta)$ (mb/sr)
100
10
1
0
30
60
90
120
150
120
θ (deg)

Fig. 12

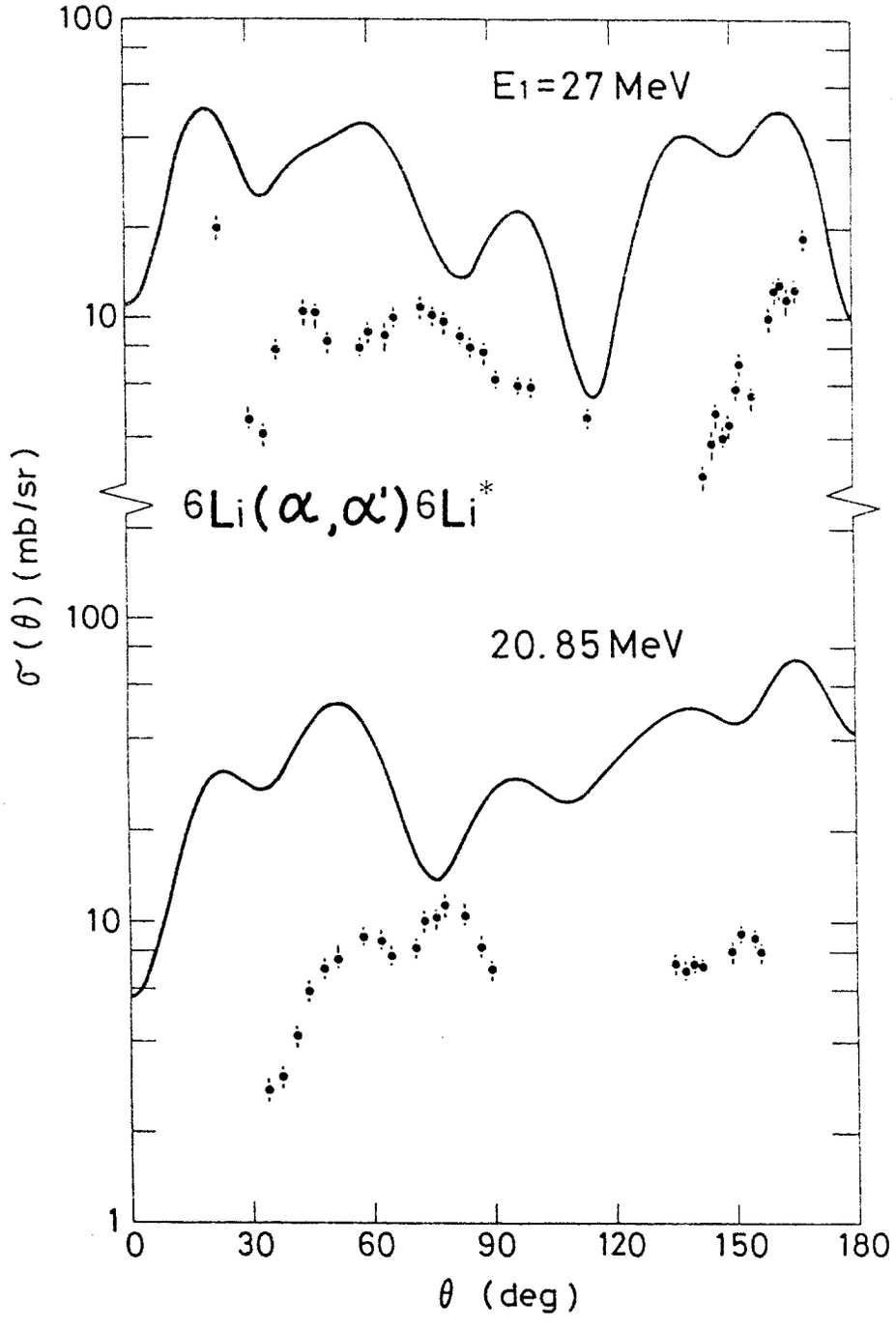
100
E1=27 MeV
10
6Li(α,α')6Li*
100
20.85 MeV
10
1
σ(θ) (mb/sr)
0
30
60
90
120
150
180
θ (deg)

Fig. 13